NUMERICAL STUDY ON COOLING PERFORMANCE AND THERMAL STRESS CHARACTERISTIC OF AN F-CLASS GAS TURBINE STATOR BLADE

Lei Xi*, Qicheng Ruan, Yuan Gao, Jianmin Gao, Liang Xu, Yunlong Li

School of Mechanical Engineering, Xi'an Jiaotong University, Xi'an 710049, Shaanxi, China

* Corresponding author; E-mail: xilei100@mail.xjtu.edu.cn

In this study, a coupled numerical computation approach integrating aerothermal and thermomechanical effects was employed to investigate the cooling efficiency and thermal stress characteristics of gas turbine stator blades. A comprehensive analysis was conducted considering varying turbulence intensities in the coolant flow (spanning from 0.05 to 0.15) and different coolant media configurations, including pure air, dual-medium mixture of air and steam, and pure steam. The distributional traits of cooling efficiency and thermal stress on the stator blade surface under these conditions were meticulously examined. Furthermore, quantitative assessments were performed to determine the extent to which coolant turbulence intensity and coolant type affect the average cooling efficiency and maximum equivalent thermal stress of turbine stator blades, thereby revealing the influence laws. The results reveal that the minimum cooling efficiency on the stator blade surface predominantly occurs at the position of channel 4 on the pressure surface, while the highest cooling efficiency is generally found near the leading edge of the suction surface. Regions of elevated thermal stress were consistently concentrated around the stator blade tip and root areas. When the coolant turbulence intensity increased from 0.05 to 0.15, the average cooling efficiency on the stator blade surface improved by 2.06%, accompanied by a reduction of 1.12% in the maximum thermal stress. In comparison to pure air cooling, dual-medium (air and steam) cooling and pure steam cooling lead to respective enhancements in the average cooling efficiency of approximately 3.3% and 13.2%, with corresponding decreases in the maximum thermal stress of 2.18% and 10.2%.

Key words: *gas turbine, turbine stator blade, cooling efficiency, thermal stress, numerical calculation*

1. Introduction

With the continuous advancement and increase in thermal efficiency and output power of modern gas turbines, the inlet temperatures of gas turbines significantly surpass the thermal endurance limits of metallic materials of blades [1]. Insufficient cooling capacity leading to high temperatures and uneven cooling causing high thermal stresses can severely impact the safe and stable operation of gas turbine blades, potentially shortening the gas turbine's lifespan [2]. Consequently, there arises an imperative need to develop sophisticated cooling technologies to regulate the temperature and thermal

stress levels within gas turbine stator blades [3], thereby ensuring their safe and reliable operations.

In the study of cooling efficiency of gas turbine stator blades, at present, the majority of gas turbine blades rely on air-based cooling techniques [4]. However, conventional air-cooling technology for gas turbine stator blades encounters issues such as low cooling efficiency, high cooling air consumption, and increasing complexity of cooling structures [5]. The use of air as the coolant medium fails to meet the demanding requirements of high-performance stator blades of heavy-duty gas turbines [6]. On the other hand, steam offers benefits of high heat capacity and superior heat transfer coefficients, which can notably enhance the cooling efficiency gas turbine stator blades. Research by Xu et al. [7] revealed that to attain equal cooling efficacy, only 48.2% of the air mass flow rate is required when employing steam as the coolant. Consequently, in order to break through the limitations of traditional cooling technologies of gas turbine stator blade and to propel the development of the next generation of advanced heavy-duty gas turbines, the integration of steam cooling and air cooling as dual-medium cooling, as well as the pure steam cooling, have become a central focus and forefront in the research of advanced cooling technologies for high-performance gas turbine stator blades [8].

In the research on the cooling effect of steam cooling in gas turbine stator blades, Wang et al. [9] conducted experimental and computational studies on internal steam convective cooling effect in a gas turbine stator blade. Their findings revealed that steam cooling exhibits a significantly higher cooling effectiveness, approximately 12% more than air cooling, particularly pronounced at the blade's mid-chord areas. Then they conducted a study on the cooling efficiency of a gas turbine stator blade equipped with a novel combined cooling structure, which integrates external film cooling and internal convection cooling using superheated steam instead of traditional compressor air [10]. They reported that the cooling effectiveness of the newly designed stator blade is higher and more evenly distributed. Shukla et al. [11] combined steam injection with film cooling in their investigation of the cooling performance and thermal efficiency of a gas turbine. Their findings indicated that steam film cooling enhances both the cooling efficiency of the stator blade and the thermal efficiency of the gas turbine. Elwekeel et al. [12] examined the effects of integrating mist into steam as a coolant medium within a steam-injected gas turbine cycle. They observed that at reduced mist temperatures, the absorption of heat by the coolant is notably augmented, consequently leading to an improvement in the blade surface temperature when steam is fortified with mist. Du et al. [13] studied how aerodynamic parameters affect steam vortex cooling in gas turbine blade leading edges. Their research showed that increasing steam velocity intensified heat transfer and reduced friction, while increasing temperature ratio led to slight heat transfer decline and substantial friction drop. Kotowicz et al. [14] carried out a study on the economic and thermodynamic properties of a combined cycle power plant featuring steam cooled gas turbine blade. Their findings revealed that the cooling efficiency of gas turbines utilizing steam as a coolant exceeds that of their air-cooled counterparts even at comparably low compression ratios. Vadlamudi et al. [15] modeled a gas turbine to compare the effects of different steam cooling methods on its performance. The results indicated that for this turbine blade, internal steam cooling and steam film cooling have higher cooling efficiency and lower entropy production compared to air cooling. Norheim et al. [16] conducted a numerical study comparing the cooling effectiveness of compressed air and steam in a gas turbine stator blade. The results showed that the SST k-ω turbulence model is better suited for numerical simulations of gas turbine blade cooling, particularly when steam is employed as the cooling medium. Zhao et al. [17] numerically examined the cooling efficiency of a

steam-cooled gas turbine stator blade. Their findings indicate that, in contrast to the air-cooled blade under various conditions, the steam-cooled blade demonstrates 18.47-29.01% increased temperature non-uniformity and 14.06-17.81% higher cooling efficiency.

In the realm of thermal stress research concerning gas turbine stator blades, several scholars have engaged in pertinent studies utilizing experimental and numerical simulation methodologies. Amaral et al. [18] developed a coupled thermal conduction model, which they employed to compute the temperature and thermal stress distributions within the gas turbine stator blade. Using the Larson-Miller parameter model, they estimated the service life of the gas turbine stator blade under creep damage. Nekahi et al. [19] undertook a numerical examination to confront the challenges of heat transfer and thermal stress in gas turbine stator blades fabricated from HfB2. They stated that HfB2 is a promising and durable material choice for turbine blade production, which demonstrates resilience against compressive stresses. Vaferi et al. [20] conducted simulations to assess TiB2's suitability for gas turbine stator blades. They determined that TiB2 can enhance the displacement limits, ensure a more uniform temperature distribution, and reduce the thermal stress compared to conventional alloys. Rahimi et al. [21] analyzed stress on a GE-F9 second stage turbine blade under uneven heating. They reported that the semi-cooling state caused the highest stress near the blade root, while full cooling led to greater stress away from the root. Rayapati et al. [22] researched the mechanical properties of different Nickel-based superalloys for gas turbine blades under great thermal loads. They found that Mar-M-200 exhibits lower deformation, stress, and strain, making it structurally stronger. Cai et al. [23] performed a thermal-fluid-solid coupling analysis on the distributions of temperature and thermal stress for a gas turbine stator blade made of Nickel-Based superalloy. They suggested that optimized cooling designs and thicker TBC layers can mitigate high temperatures and great temperature gradients, thereby reducing the thermal stress in the gas turbine stator blade.

Although the above reviewed literature have preliminarily researched the cooling performance of gas turbine stator blades using steam cooling and dual-medium cooling with air/steam, as well as the distribution of thermal stress, few studies have integrated a comprehensive examination of both cooling efficiency and thermal stress of gas turbine stator blades. Especially, there has been no literature yet conducting a comprehensive study on the distribution patterns of cooling efficiency and thermal stress under varying coolant turbulence intensities and coolant mediums.

In response to the deficiencies in the existing literature, this study focuses on a dual-medium cooled turbine stator blade designed in our laboratory [24], conducting a comprehensive investigation into the cooling efficiency and thermal stress under coolant turbulence intensity ranging from 0.05 to 0.15, and utilizing coolant mediums comprising pure air, mixture of air and steam, and pure steam. Firstly, the distribution characteristics of the cooling efficiency on the stator blade surface under varied coolant turbulence intensity and coolant types were deeply investigated. Subsequently, the distribution properties of thermal stress in the turbine stator blade were thoroughly examined. Finally, the extent to which coolant turbulence intensity and coolant type affect the average cooling efficiency and maximum equivalent thermal stress of the turbine stator blade was quantified, thus deriving corresponding influencing patterns.

2. Research object and numerical calculation methods

2.1. Research object

The research object of this study is a dual-medium (air/steam) cooled turbine stator blade designed within our laboratory [24], which has been geometrically scaled down by a factor of 0.5 based on the mid-section profile of an actual first-stage stator blade from a specific F-class gas turbine. The stator blade chord length measures 126 mm, and its height stands at 83 mm, featuring an inlet angle of 107° and an exit angle of 17°. As depicted in Figure 1, the stator blade's structural schematic shows the presence of four distinct cooling cavities. Channel 1 serves as the supply for film cooling at the leading edge, whereas channel 4 caters to the trailing edge convective hole cooling. Intermediate channels 2 and 3 are utilized for internal rib cooling. Specifically, the structures of channels 2 and 3 are similar, each with a rib angle of 90°, a rib pitch of 25 mm, and a rib height of 2.5 mm. In the original dual-medium cooled turbine stator blade as presented in Reference [24], a dual-medium cooling with air/steam was employed, where channels 1 and 4 are cooled by air, while channels 2 and 3 are cooled by steam. In the present study, in addition to this original dual-medium cooling scheme, comparisons are made with pure air cooling, where all four channels are cooled by air, and pure steam cooling, where each of the four channels utilizes steam as the cooling medium.

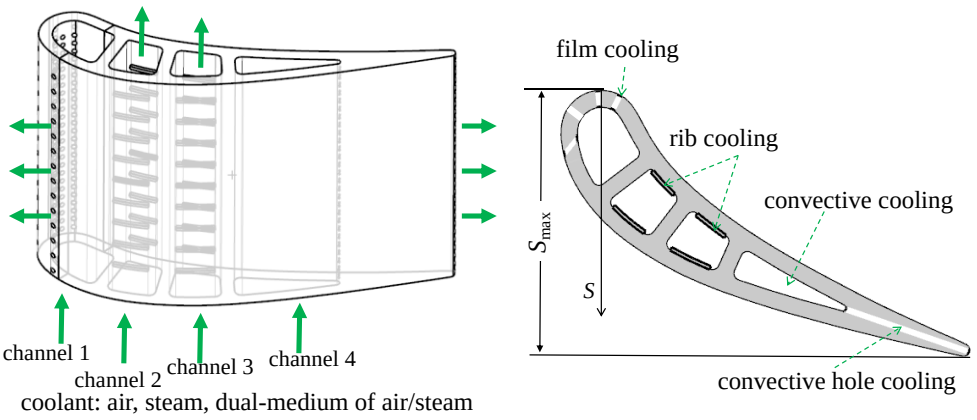

Fig. 1 Geometric model

2.2. Calculation methods for flow and heat transfer

Figure 2 illustrates the numerical calculation model for the gas turbine stator blade, encompassing inlet and outlet fluid rectification sections, mainstream flow computational domain, cooling channel fluid computational domain, and the solid stator blade computational domain. In numerical calculations, the fluid was assumed to be a 3D, compressible, gravity independent turbulent flow. The finite element-based finite volume method was used to discrete the control equations, and a fully implicit coupled multigrid approach was adopted. The three-dimensional compressible Reynolds-averaged Navier-Stokes equations were solved using the CFX solver, with turbulent flow phenomena modeled by the *k-ε*, *k-ω*, and SST *k-ω* transitional turbulence models to compute the fluid temperature. High-order accurate discretization schemes were employed for the diffusion terms, source terms, and convection terms, achieving a global residual convergence level of 10^{-6}.

The mainstream computational domain was set as a single passage of the turbine stator blade row, with periodic boundaries on both sides of the mainstream passage, and adiabatic boundaries on

the upper and lower walls of the mainstream passage. Along the axial direction of the stator blade, an upstream extension of one stator blade chord length ahead of the leading edge and a downstream extension of the same length behind the trailing edge served as the positions for setting the boundary conditions, respectively. To better assess the heat transfer characteristics of the stator blade, fluid-solid coupling boundary conditions were implemented between the gas-side and coolant-side fluid flows and the solid conduction within the stator blade. This ensures a comprehensive evaluation of the heat transfer properties and interactions occurring between the fluid and solid domains.

In the numerical calculations, the mainstream fluid and the cooling air were modeled as ideal compressible air closely approximating real operating conditions, with their material properties being adjusted according to ideal gas parameters provided within the CFX software. The dynamic viscosity and thermal conductivity of the air were determined using the Sutherland formula [25]. The specific heat capacity of air, denoted by c_p, was approximated using a linear temperature-dependent equation: $c_p = 0.2348T + 936.95$, $J \cdot kg^{-1} \cdot K^{-1}$. Regarding the cooling steam, the corresponding cooling fluid material properties were set according to the IAPWS-IF97 for water and steam properties. The stator blade material was stainless steel 304, with a density of $\rho = 7930$ kg/m³. The thermal conductivity of this stainless steel, k, was also temperature-dependent, given by $k = 0.0095T + 14.06$, $W \cdot m^{-1} \cdot K^{-1}$.

The computational grid of the stator blade used in this study is illustrated in Figure 3, where the entire computational domain is comprised of structured multi-block grids. To enhance grid quality, local grid refinement was carried out in the vicinity of the fluid-solid interfaces and the wall regions of both the fluid domain and the stator blade solid domain. The distance from the first layer of grid elements to the wall surface was set to 0.001 mm, and a growth ratio of 1.2 was employed to ensure that the $y+$ value in the heat transfer regions remained less than 1, thereby accurately capturing the near-wall effects. For the reliability and precision of the numerical method, a grid independence study have been conducted for the cooling numerical calculation of this stator blade based on the GCI index [26]. The grid convergence study results listed in Table 1 (based on the ratio of blade surface average temperature to mainstream inlet total temperature) show that a total grid number of 4.25 million can satisfy the requirements of the grid independence study, i.e., ensuring that the results were independent of the grid numbers. This is because when the total grid number is 4.25 million, the GCI index is already very small (less than 3%), which can be considered to meet the grid independence requirements.

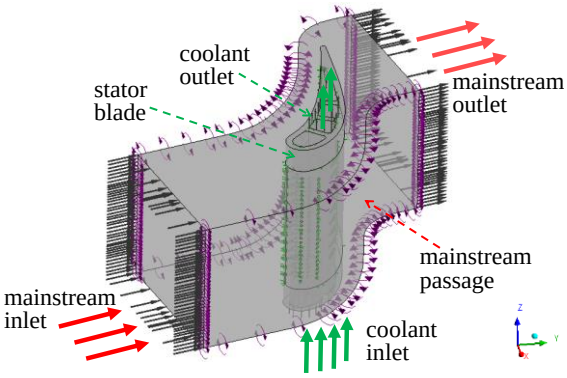

Fig. 2 Numerical model

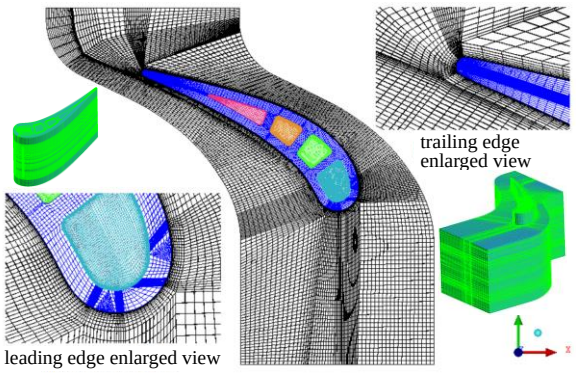

Fig. 3 Grid model

Table 1 Grid convergence study results

No.	Total Grid Number/Million	Grid Refinement Ratio	T_{ave}/T_0	GCI Index
1	2.10	-	0.753	-
2	2.50	1.19	0.747	5.44%
3	3.01	1.20	0.741	5.12%
4	3.60	1.20	0.737	3.58%
5	4.25	1.18	0.734	2.93%
6	5.00	1.18	0.732	2.01%

2.3. Calculation method for thermal stress

Utilizing the ANSYS Workbench multiphysics solution platform, the thermal stress analysis and computation of the gas turbine stator blade's solid domain were executed. The turbine stator blade was subjected to fixed constraints at its upper and lower ends. During the computations, the body temperature field of the turbine stator blade obtained from the CFD analysis was imposed as a boundary condition onto the solid domain of the turbine stator blade. Based on the generic steel material provided in the ANSYS Workbench material library, certain attributes were customized to match those of 304 stainless steel, with the relevant material properties tabulated in Table 2 [27]. The geometrical model and mesh model employed for the thermal stress calculation were consistent with those used in the CFD computations, thereby reducing potential data discrepancies when transferring the CFD results to the stress calculation process.

Table 2 Material Properties of 304 Stainless Steel

Properties	Ranges
Density/kg·m^{-3}	7930
Longitudinal modulus of elasticity /Pa	1.93×10^{11}
Linear expansion coefficient/1·K^{-1}, under temperature between 20℃ and 400℃	1.81×10^{-5}
Poisson's ratio	0.3

2.4. Parameter definition

The static pressure distribution and static temperature distribution at the mid-section of the stator blade are treated as ratios relative to the mainstream inlet total pressure and total temperature, respectively, expressed as pressure ratio (P/P_0) and temperature ratio (T/T_0).

The cooling efficiency on the stator blade surface is defined as:

$$\eta = (T_g - T)/(T_g - T_c) \tag{1}$$

where T_g is the mainstream temperature, T_c is the temperature of the cooling medium, T is the local temperature on the surface of the stator blade.

To evaluate the overall cooling efficiency of the entire stator blade surface, the concept of average cooling efficiency is introduced, and its calculation formula is given as follows:

$$\overline{\eta} = (T_g - T_a)/(T_g - T_c) \tag{2}$$

where T_a represents the average temperature across the entire stator blade surface.

Thermal stress resolution typically relies on the theory of linear thermal stress [28]. This theory posits that when a temperature change occurs, an object develops stress due to restraint, and such stress arises from the superposition of two components: one part is proportional to the temperature change and manifests as stress in all directions [29], while the other part comprises the stress generated by strain without considering temperature effects. Thus, the stress is divided into two parts:

$$\begin{cases} \sigma_x = \sigma_x' - \beta\Delta T \\ \sigma_y = \sigma_y' - \beta\Delta T \\ \sigma_z = \sigma_z' - \beta\Delta T \end{cases} \tag{3}$$

where β is the thermal stress coefficient, σ_x, σ_y, and σ_z are the total stress in the *x*, *y*, and *z* directions, σ_x', σ_y', and σ_z' are the stress generated by strain in the *x*, *y*, and *z* directions.

For steady-state solutions, thermal stress primarily arises from non-uniform temperature distributions (i.e., temperature gradients) within the object's various parts. In a Cartesian coordinate system, the temperature gradient in the solid domain can be calculated using the following formula:

$$\nabla T = \frac{\partial T}{\partial x}\vec{i} + \frac{\partial T}{\partial y}\vec{j} + \frac{\partial T}{\partial z}\vec{k} \tag{4}$$

where $\frac{\partial T}{\partial x}$, $\frac{\partial T}{\partial y}$ and $\frac{\partial T}{\partial z}$ are the partial derivatives of temperature in the *x*, *y*, and *z* directions, respectively, $\vec{i}$, $\vec{j}$ and $\vec{k}$ are the unit vectors in the *x*, *y*, and *z* directions, respectively.

3. Validation of numerical methods

In this paper, three widely-used turbulence models—*k*-*ε*, *k*-*ω*, and SST *k*-*ω*—were employed to numerically simulate the stator blade cooling and perform mesh reliability verification. Figures 4(a) and 4(b) illustrate the distribution curves of static pressure and temperature along the stator blade surface at the mid-section relative to the chord length, where the vertical axes represent the ratio of stator blade surface local static pressure to mainstream gas inlet total pressure (P/P_0) and the ratio of stator blade surface local temperature to mainstream gas inlet temperature (T/T_0), respectively. The horizontal axis denotes the dimensionless chord length (S/S_{max}), where S/S_{max} = 0 represents the stagnation point at the stator blade leading edge, S/S_{max} = 1 signifies the position of the last point on the trailing edge, S/S_{max} < 0 corresponds to the pressure surface, and S/S_{max} > 0 refers to the suction surface.

Figure 4 shows a comparison of the predicted values from the three turbulence models against the experimental values from Reference [24]. From Figure 4(a), it can be seen that all turbulence models provide good agreement with the experimental results regarding the static pressure distribution on the stator blade surface, albeit with slightly underestimated predictions near the trailing edge on the suction surface. In Figure 4(b), it is evident that for the pressure surface close to the trailing edge, the predicted stator blade surface temperatures from the three models are higher than the experimental values, with the largest deviation occurring at S/S_{max} = -0.73. In the middle region of the pressure surface, the predicted temperatures from the three models are relatively close to the experimental values, with the maximum prediction error not exceeding 6%. At the stator blade leading edge, the *k*-*ω*

and SST *k-ω* models yield temperature predictions that closely align with the experimental values, while the *k-ε* model exhibits larger deviations. On the suction surface, the SST *k-ω* model provides the most accurate predictions, with errors staying within 3%. Overall, the SST *k-ω* turbulence model demonstrates the closest agreement with the experimental values among the three models. Hence, for subsequent numerical calculations in this paper, the SST *k-ω* turbulence model will be adopted.

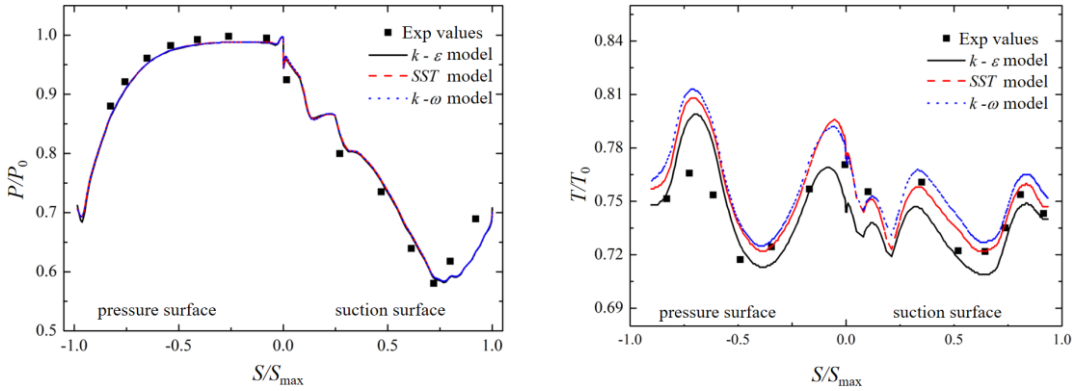

(a) static pressure distribution on blade surface (b) temperature distribution on blade surface

Fig. 4 Numerical method validation based on experimental data in Reference [24]

4. Result analysis and discussion

In this paper, the mainstream operating conditions, coolant inlet temperature and coolant outlet conditions are kept constant, so as to intensively analyze the effects of coolant turbulence intensity and coolant type on the cooling efficiency distributions and solid thermal characteristics of the gas turbine stator blades. Variations were introduced solely in terms of coolant inlet turbulence intensity and coolant composition (pure air, a dual-medium of air/steam, and pure steam). The detailed working condition setups are presented in Table 3.

Table 3 Working conditions

Parameters	Values
Mainstream inlet total temperature/K	633
Mainstream inlet total pressure/kPa	188
Mainstream inlet turbulence intensity	0.05
Mainstream inlet-outlet pressure ratio	1.5
Coolant inlet total temperature/K	298
Coolant inlet total pressure/kPa	201
Coolant inlet turbulence intensity	0.05 to 0.15
Coolant medium	pure air, a dual-medium of air/steam, and pure steam

4.1. Flow field distribution

Taking dual-medium cooling with air/steam as an example, Figure 5 presents the 3D flow field distributions within the mainstream passage and cooling channels, along with a 2D flow field

distribution map formed by the cooling fluid. Specifically, Figure 5(a) and 5(b) illustrate the 3D flow field distributions on the pressure and suction sides, respectively. Figures 5(c) and 5(d) depict the 3D vortex core distributions around the stator blade on both the pressure and suction sides; these vortex cores are generated using CFX's built-in λ_2 criterion [30]. Figure 5(e) shows the flow field distribution of the cooling fluid.

From Figures 5(a) and 5(b), it is evident that the velocity of the cooling fluid in channels 1 and 4 is relatively low, as these fluids must mix with the mainstream through film holes and trailing edge convective holes. Conversely, the cooling fluid in channels 2 and 3, which is directly discharged from the cooling channel outlets, has a higher velocity. The velocity of the mainstream initially increases and then decreases from the mainstream inlet to the mainstream outlet on both the pressure and suction sides. The maximum velocity of the mainstream on the suction side is reached approximately at the location of channel 3, whereas on the pressure side, this peak occurs after the blade's trailing edge.

Figures 5(c) and 5(d) reveal that on the pressure side, vortices with smaller size and slower velocity primarily form around the film holes and trailing edge convective holes. On the suction side, continuous distributions of vortices with larger size and faster velocity develop around these holes and their downstream. Notably, large, high-speed vortices also form in the downstream region of the blade's trailing edge. These vortices have a notable impact on the temperature distribution and cooling efficiency of the blade surface.

From Figure 5(e), it is observed that as the cooling fluid from channel 1 enters the film holes, its velocity increases due to a sudden decrease in cross-sectional area. The cooling fluid then sprays into the mainstream, forming a film on the blade surface. Under the influence of the mainstream, the velocity of the film first decreases and then increases on the pressure side. On the suction side, the film adheres closely to the blade surface, rapidly increasing in speed until it undergoes transition between channels 3 and 4, reaching a maximum velocity before gradually decreasing again. Additionally, there is a noticeable poor coverage of the film on the pressure side between the leading edge and channel 2, which may result in inferior cooling performance in this area. In contrast, except for a local region at the leading edge, the film coverage on the suction side is generally better, contributing to enhanced cooling effectiveness on this side.

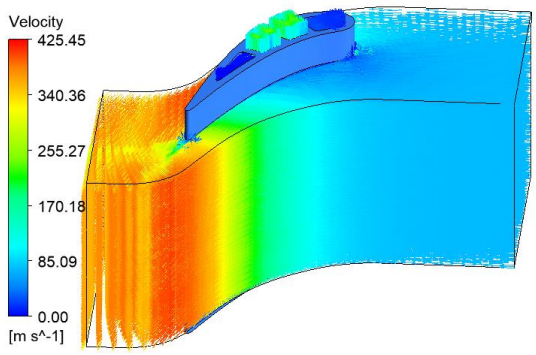

(a) 3D flow field on pressure surface side

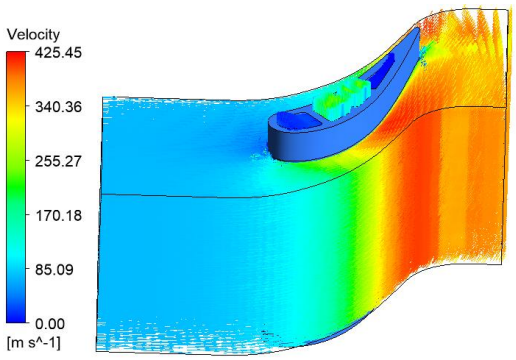

(b) 3D flow field on suction surface side

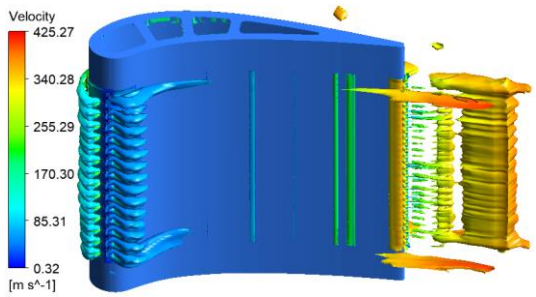

(c) 3D vortex core on pressure surface side

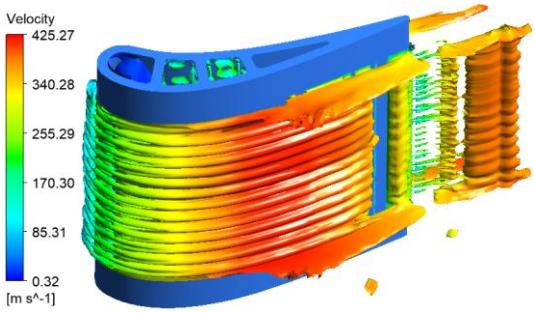

(d) 3D vortex core on suction surface side

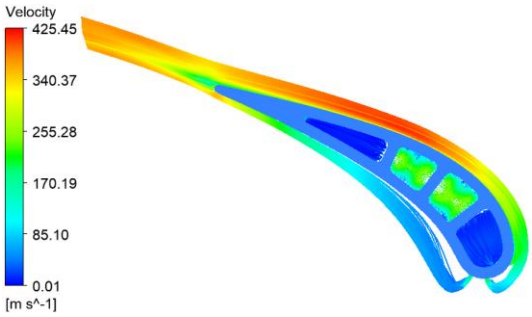

(e) flow field of cooling fluid

Fig. 5 Distribution characteristics of flow field in mainstream passage and cooling channel

4.2. Cooling efficiency distribution

Taking dual-medium cooling with air/steam as an example, Figure 6 presents the distribution contour maps of cooling efficiency on the stator blade pressure and suction surfaces under a turbulence intensity of 0.05 and the dual-medium cooling. Initially, observing from the mainstream flow direction, the leading edge of the stator blade, despite being equipped with film cooling, experiences poor cooling efficiency due to direct exposure to the high-temperature mainstream. Subsequently, within the areas of channels 2 and 3, enhanced cooling efficiency is evident due to the presence of rib turbulators, and the relatively larger coolant flow rates in channels 2 and 3, alongside better film cooling effectiveness. Thereafter, in the zone of channel 4, a decline in cooling performance is observed, mainly due to its simpler internal convective cooling configuration, with a more pronounced drop in cooling efficiency on the pressure surface. Lastly, towards the trailing edge, the cooling efficiency improves because of the densely arranged convective cooling holes as well as a decrease in static gas temperature caused by the effects of mainstream acceleration.

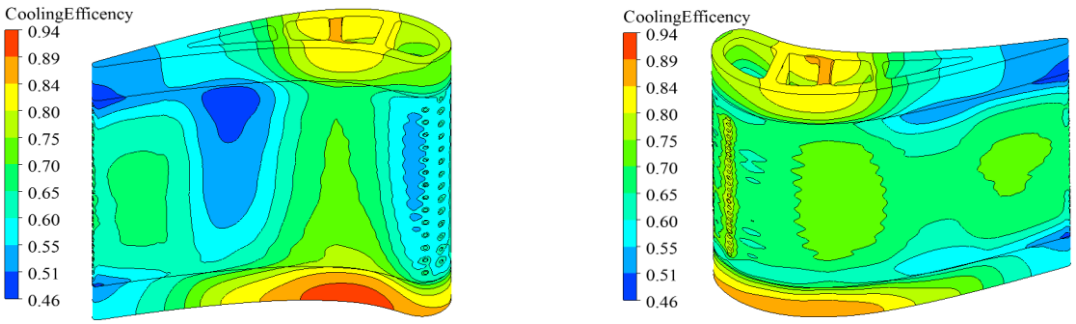

(a) cooling efficiency on pressure surface (b) cooling efficiency on suction surface

Fig. 6 Distribution characteristics of cooling efficiency on the surface of turbine stator blade

Additionally, it is evident from Figure 6 that the cooling efficiency on the pressure surface of the stator blade is lower than that on the suction surface. This is attributed to the lower static pressure and higher velocity of the mainstream on the suction surface, resulting in a lower static temperature and thus higher cooling efficiency on the suction surface. Furthermore, the cooling efficiency distribution along the stator blade height is not symmetrical, with noticeably lower cooling efficiency near the stator blade tip on both the pressure surface and suction surface compared to those near the stator blade root. This asymmetry is related to the coolant ingress from the stator blade root. Upon examining the entire Figure 6, it is clear that the stator blade's lowest cooling efficiency predominantly occurs at the position of channel 4 on the pressure surface. Moreover, low cooling efficiency is also observed near the film cooling holes on the pressure surface close to the leading edge. Besides, low cooling efficiency is also observed in localized regions on both the pressure surface and suction surface near the trailing edge, with a larger low-cooling-efficiency area at the stator blade tip. In contrast, the highest cooling efficiency is predominantly found at the locations between channels 2 and 3 on the pressure surface and suction surface, specifically, in the vicinity of channel 2 on the pressure surface near the stator blade root, where cooling efficiency is relatively high.

In general, a turbulence intensity of 0.05 is considered moderate, while values above 0.1 denote high turbulence intensity. In this study, numerical simulations were performed with coolant inlet turbulence intensities ranging from 0.05 to 0.15, taking dual-medium cooling with air/steam as an example. Figure 7 presents distribution contour maps of stator blade surface cooling efficiency under different coolant inlet turbulence intensities. From Figure 7, it can be discerned that the coolant inlet turbulence intensity has a negligible effect on the distribution pattern of cooling efficiency on the stator blade surface with the specific cooling structure studied herein. Regardless of the coolant type, poorer cooling performance is consistently observed in the leading edge region as well as the pressure surface at channel 4, while more effective cooling takes place in the regions of channels 2 and 3, as well as the trailing edge. Moreover, Figure 6 demonstrates that when the coolant turbulence intensity increases from a moderate level (0.05) to a high level (0.1), there is a noticeable enhancement in the cooling efficiency across the stator blade surface, particularly in the pressure surface and suction surface of the area near channel 2, where the improvements are most pronounced. However, upon further escalation of the coolant turbulence intensity from 0.1 to 0.15, minimal changes occur in the stator blade surface cooling efficiency. Closer analysis reveals that an increase in inlet coolant turbulence intensity signifies a heightened magnitude of fluctuating velocity in the cooling fluid, which in turn leads to a more chaotic flow within the cooling channels. This augmented turbulence

intensity enhances heat transfer in the cooling channels and, consequently, improves the cooling efficiency of the gas turbine stator blade. This finding suggests that, beyond a coolant turbulence intensity of 0.1, increasing coolant turbulence intensity contributes very little to enhancing the cooling effect on the stator blade surface. Therefore, a coolant turbulence intensity of 0.1 is deemed a suitable coolant inlet turbulence level for the cooling of gas turbine blade.

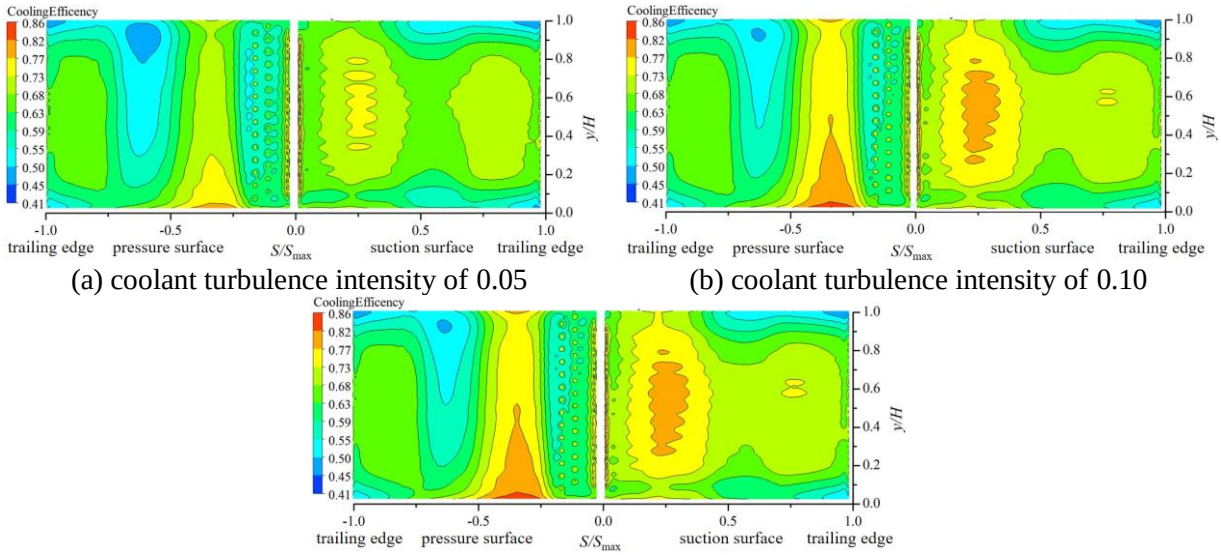

(a) coolant turbulence intensity of 0.05 (b) coolant turbulence intensity of 0.10

(c) coolant turbulence intensity of 0.15

Fig. 7 The influence of coolant turbulence intensity on the distribution of stator blade surface cooling efficiency under dual-medium cooling

Figure 8 presents distribution contour maps of stator blade surface cooling efficiency during cooling with the three selected coolant mediums: pure air, a dual-medium consisting of air and steam, and pure steam, under a coolant turbulence intensity of 0.10. The results in Figure 8 indicate that the distribution pattern of cooling efficiency on the stator blade surface with the specific cooling structure under this study remains largely unaffected by the choice of coolant. Notably, compared to pure air cooling, dual-medium cooling with air/steam exhibits a more significant enhancement in stator blade surface cooling efficiency. Further, when switching from pure air cooling to pure steam cooling, there is a pronounced increase in cooling efficiency, especially evident on the suction surface of the stator blade. As gleaned from Figure 8, the dual-medium cooling with air/steam only significantly improves cooling efficiency in the mid-chord region compared to pure air cooling, without appreciable gains in the leading edge and trailing edge regions. This is due to the fact that steam is only introduced in channels 2 and 3 within the mid-chord area of the stator blade, while channels 1 at the leading edge and channel 4 at the trailing edge continue to utilize air for cooling purposes. This observation underscores the limited impact of mid-chord steam cooling on the leading edge and trailing edge. For the pure steam cooling, which supplies steam to all four channels, leads to a substantial improvement in cooling performance across the entire stator blade surface relative to pure air cooling.

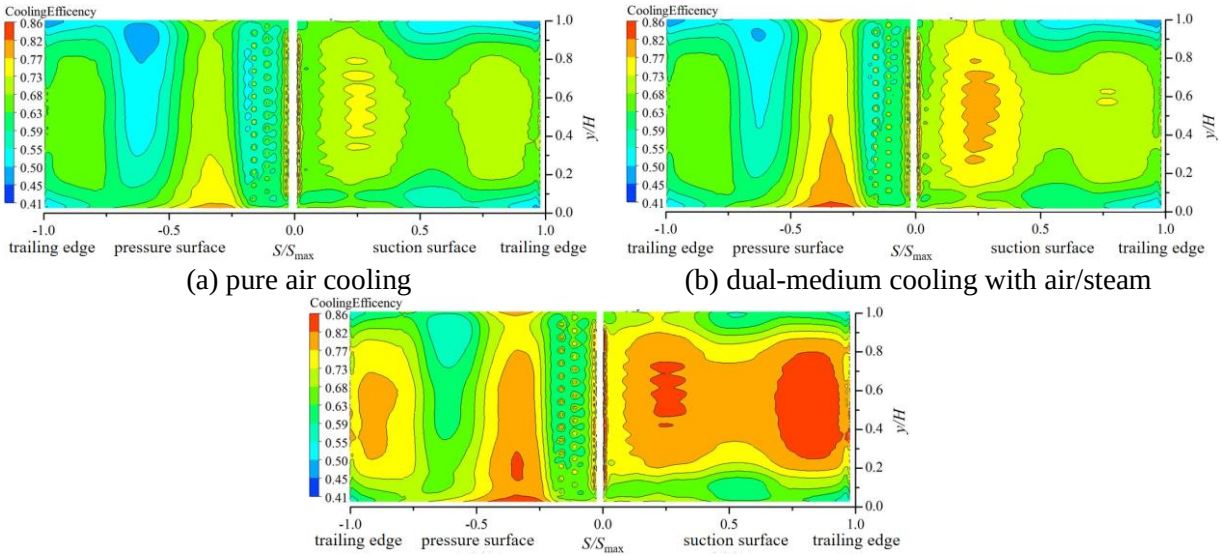

(a) pure air cooling (b) dual-medium cooling with air/steam

(c) pure steam cooling

Fig. 8 The influence of cooling medium on the distribution of stator blade surface cooling efficiency under coolant turbulence intensity of 0.10

4.3. Solid thermal characteristic distribution

Based on the preceding analysis, it is evident that coolant turbulence intensity and coolant type exert an influence on the values of the cooling efficiency of the turbine stator blade, yet they have minimal impact on the distribution characteristics of the cooling efficiency. Consequently, in this subsection, focusing on dual-medium cooling with air/steam as an example, a comprehensive analysis of the solid thermal characteristics of the turbine stator blade is undertaken under a coolant turbulence intensity of 0.1. Figure 9 presents distribution contour maps of temperature gradient, local displacement (deformation), and thermal stress on the surface of the dual-medium cooled turbine stator blade. From Figures 9(a) and 9(b), it can be discerned that along the mainstream flow direction, the temperature gradient is significantly higher at both the stator blade leading edge and trailing edge, while in the blade height direction, greater temperature gradients are observed in the vicinity of the stator blade root and tip regions, with the smallest temperature gradient occurring at the middle region in the mid-chord area of the suction surface.

Figures 9(c) and 9(d) reveal that, along the stator blade height direction, deformation is more pronounced in the mid-height region compared to the stator blade tip and root locations, mainly due to the fixed constraints at the stator blade tip and root that limit the deformation. Additionally, from the perspective of the mainstream flow direction, larger deformations are found in the leading edge and trailing edge regions, potentially linked to the higher temperature gradients in these areas. Also notable is that deformation levels are higher in the mid-chord region of the suction surface compared to the corresponding pressure surface region, possibly related to the respective geometric structure form of the pressure surface and suction surface.

Figures 9(e) and 9(f) demonstrate that regions of higher thermal stress are concentrated around the stator blade tip and root areas, likely due to the fixed constraints imposed at the stator blade's top and bottom ends, which restrict deformation associated with temperature variations in these zones and thereby yield higher thermal stress. Furthermore, for the top and bottom ends of the stator blade, they display heightened thermal stress at its leading edge and trailing edge, with lower stress levels in the

mid-chord region. This is attributable to the fact that, for the stator blade's top and bottom ends, the mid-chord region's material has a greater freedom to expand or contract sideways compared to the leading and trailing edges, which have limited room for such deformation. The minimum equivalent stress value is located at the leading edge film cooling holes and trailing edge convection cooling holes, with a value of 2.80×10^{7} Pa, while the maximum equivalent stress value is found at the blade ends of the trailing edge region, reaching 4.37×10^{9} Pa.

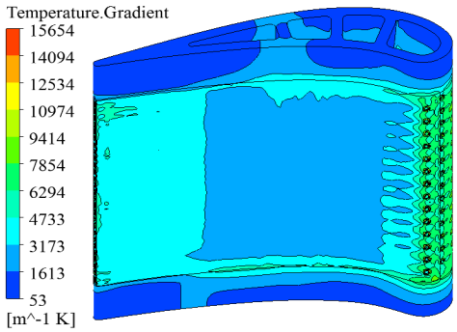

(a) temperature gradient of pressure surface

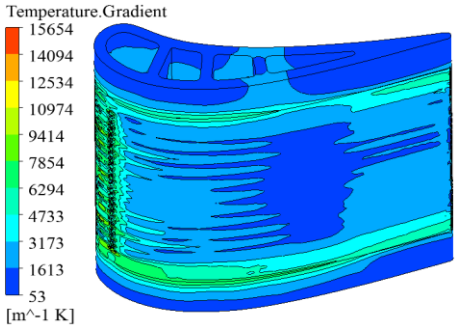

(b) temperature gradient of suction surface

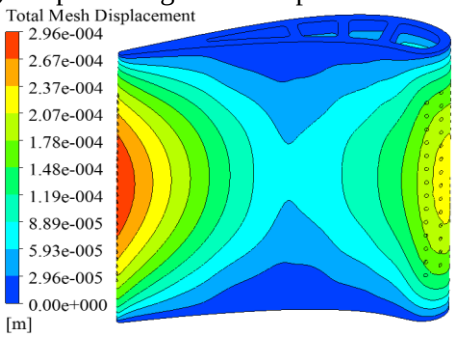

(c) local displacement of pressure surface

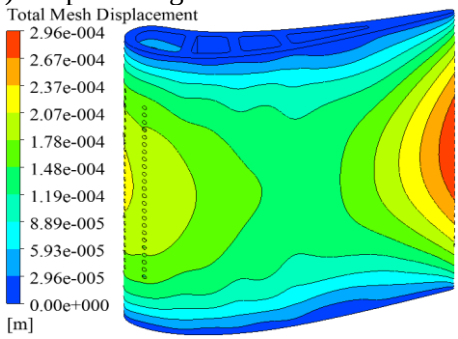

(d) local displacement of suction surface

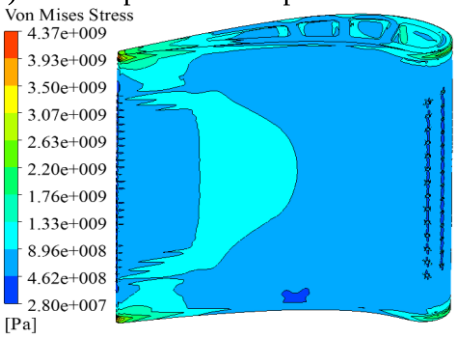

(e) equivalent thermal stress of pressure surface

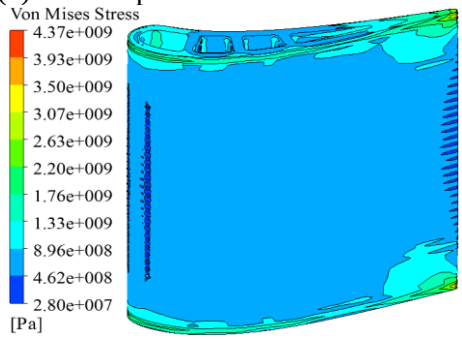

(f) equivalent thermal stress of suction surface

Fig. 9 Contour maps of temperature gradient, local displacement, and equivalent thermal stress on stator blade surface

4.4. Comprehensive analysis

To investigate the distribution characteristics of turbine stator blade deformation and thermal stress along the mainstream flow direction and their relationship with stator blade surface cooling efficiency, Figure 10 presents line graphs depicting the variation of cooling efficiency, deformation, and thermal stress across the mid-section of the turbine stator blade. Similarly, Figure 10 also takes dual-medium cooling with air/steam as an example, with a coolant turbulence intensity of 0.1. In Figure 10, the black solid line, red dashed line, and blue dotted line respectively represent the

distribution of stator blade surface cooling efficiency, stator blade deformation, and equivalent thermal stress, corresponding to the left vertical axis, the right first vertical axis, and the right second vertical axis.

From Figure 10, it can be observed that the stator blade deformation distribution curve along the stator blade mid-section follows a "W" shape, with higher values at the leading edge of the suction surface, trailing edge and partial mid-chord region. This is because these areas feature respective arrangements of film cooling, rib cooling, and trailing edge hole cooling. Conversely, regions with lower cooling efficiency, such as the stagnation point at the leading edge, experience elevated temperatures due to direct exposure to high-temperature gas main flows. Meanwhile, the area near the trailing edge exhibits higher temperatures because channel 4 lacks any implemented cooling structures. There is a positive correlation between stator blade deformation and cooling efficiency at the leading edge and trailing edge of the turbine stator blade, whereas in the mid-chord area, stator blade deformation shows a monotonous increase or decrease, while stator blade cooling efficiency exhibits fluctuations. The distribution of mid-section surface thermal stress on both the pressure surface and suction surface of the turbine stator blade resembles an "M" shape, and generally follows an inverse pattern to that of cooling efficiency, which exhibits a "W" shape on both pressure and suction surfaces. This suggests that, under the current stator blade configuration, there exists a negative correlation between thermal stress and cooling efficiency along the spanwise direction in the middle region of the stator blade, i.e., positions with higher cooling efficiency exhibit lower thermal stress levels. The underlying reason could be that when the stator blade is fixed at both its top and bottom ends, the middle spanwise region experiences weaker constraints, making temperature the dominant factor affecting the stator blade's stress field in this area. Since the stator blade surface temperature and cooling efficiency are negatively correlated, the thermal stress and cooling efficiency display a negative correlation in this region.

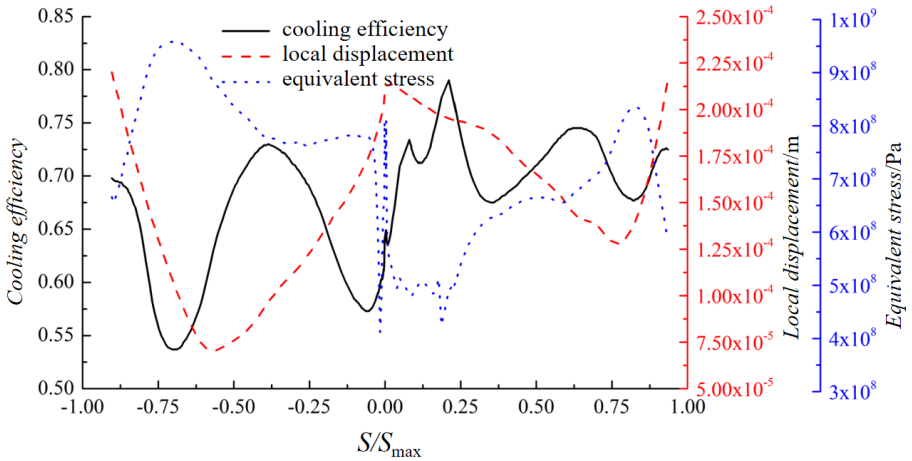

Fig. 10 Curve plot of surface cooling efficiency, local displacement, and equivalent stress on stator blade cross-section

Figure 11 presents the distribution curves of the average cooling efficiency and maximum thermal stress on the turbine stator blade surface for different coolant inlet turbulence intensities and cooling media, where solid lines represent the average cooling efficiency, and dashed lines correspond to the maximum thermal stress. As shown in Figure 11(a), the average cooling efficiency on the stator blade surface increases as the coolant inlet turbulence intensity grows, while the maximum thermal

stress decreases progressively with the rise in coolant inlet turbulence intensity. This phenomenon occurs because an increased coolant turbulence intensity leads to more effective cooling of the stator blade, lowering its temperature and consequently diminishing its deformation. The reduced deformation results in lesser loads and strains at the stator blade's fixed constraints, thus lowering the stress levels. Calculations indicate that when the coolant turbulence intensity increases from 0.5 to 0.15, the stator blade surface's average cooling efficiency rises by 2.06%, and the maximum thermal stress drops by 1.12%.

From Figure 11(b), in comparison to pure air cooling, it is evident that both dual-medium cooling with air/steam and pure steam cooling significantly enhance the average cooling efficiency of the stator blade surface and lead to a marked reduction in the maximum thermal stress. This outcome of lower thermal stress is attributed to the superior cooling efficiency and more thorough, uniform cooling effect achieved by dual-medium cooling with air/steam and pure steam cooling as compared to pure air cooling. The computed results show that, relative to pure air cooling, dual-medium cooling with air/steam and pure steam cooling elevate the average cooling efficiency of the stator blade surface by approximately 3.3% and 13.2%, respectively, while decreasing the maximum thermal stress by 2.18% and 10.2%, respectively. In summary, the increase in coolant turbulence intensity not only enhances cooling performance but also diminishes thermal stress on the gas turbine stator blade surface. Replacing pure air cooling with pure steam cooling confers cooling advantages not only in terms of the stator blade surface cooling efficiency but also in terms of the stator blade's thermal stress levels.

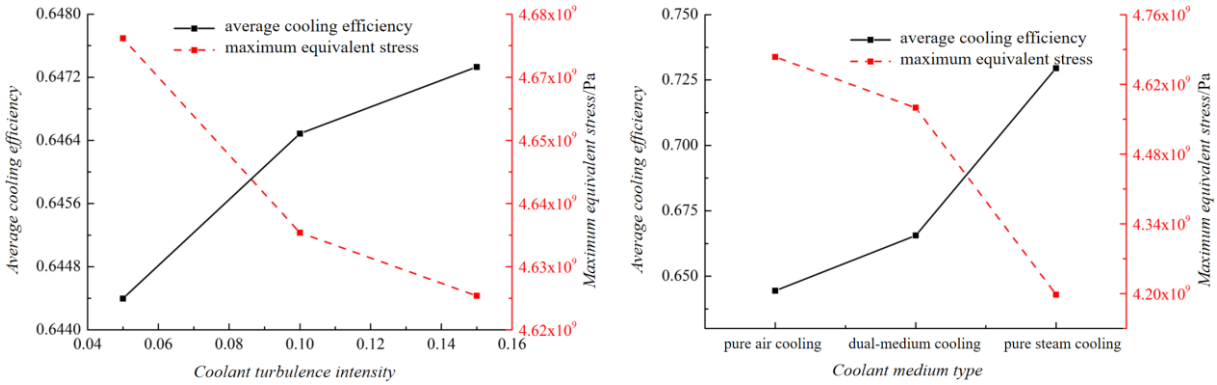

(a) coolant turbulence intensity (b) coolant medium

Fig. 11 Variation patterns of the average cooling efficiency and maximum equivalent stress on the stator blade surface under different conditions

5. Conclusions

In this study, a coupled numerical computation methodology integrating aerothermal and thermomechanical effects was employed to conduct a joint investigation into the cooling efficiency and thermal stress of gas turbine stator blades. The influence patterns of coolant turbulence intensity and coolant type on the average cooling efficiency and maximum equivalent thermal stress of gas turbine stator blades were analyzed, yielding the following principal conclusions:

(1) The lowest cooling efficiency on the stator blade surface is primarily observed at the location of channel 4 on the pressure surface. Conversely, the highest cooling efficiency is predominantly found in proximity to the leading edge area on the suction surface (between channels 1

and 2), with a comparably higher cooling efficiency also detected near the root section adjacent to channel 2 on the pressure surface.

(2) Regions of elevated thermal stress are concentrated around the stator blade tip and root areas, with a characteristic pattern showing higher thermal stress values at the leading and trailing edges of both stator blade ends, juxtaposed with relatively lower thermal stress in the mid-chord region.

(3) An increase in coolant turbulence intensity not only enhances cooling effectiveness but also reduces thermal stress in the stator blade. When the coolant turbulence intensity rises from 0.5 to 0.15, the average cooling efficiency on the stator blade surface improves by 2.06%, while the maximum thermal stress decreases by 1.12%.

(4) Compared to pure air cooling, dual-medium cooling with air/steam and pure steam cooling lead to approximate increases of 3.3% and 13.2% in the average cooling efficiency of the stator blade surface, respectively, accompanied by reductions of 2.18% and 10.2% in the maximum thermal stress.

(5) The adoption of either pure steam cooling or dual-medium cooling with air/steam not only boosts the cooling efficiency of turbine stator blades but also effectively mitigates the thermal stress encountered by the stator blades.

Acknowledgements

This research was funded by the Xi'an Jiaotong University Basic Research Business Fee Free Exploration Project (xzy012023071) and National Key Research and Development Program of China (2021YFF0602301).

References

[1] Bang, M., *et al.*, Augmented Cooling Performance in Gas Turbine Blade Tip with Slot Cooling, *Int. J. Heat Mass Trans.*, *201* (2023), pp. 123664

[2] Xi, L., *et al.*, Study on Flow and Heat Transfer Characteristics of Cooling Channel Filled with X-Shaped Truss Array, *Therm. Sci.*, *27* (2023), pp. 739-754

[3] Chowdhury, T.S., *et al*., A Critical Review on Gas Turbine Cooling Performance and Failure Analysis of Turbine Blades, *International Journal of Thermofluids*, *18* (2023), pp. 100329

[4] Long, Z., *et al.*, Research on Active Modulation of Gas Turbine Cooling Air Flow, *Appl. Therm. Eng.*, *230* (2023), pp. 120874.

[5] Ma, C., *et al.*, Heat Transfer Performance of Steam/Air Flow in Inverted V-shaped Rib-Roughened Channels. *P. I. MECH. ENG. A-J. POW.*, *235* (2021), 8, pp. 1933-1945

[6] Sun, N., *et al.*, An Experimental and Numerical Study on the Liquid Cooling of a Gas Turbine Blade, *Appl. Therm. Eng.*, *223* (2023), pp. 120005

[7] Xu, L., *et al.*, Experimental Study on Cooling Performance of a Steam-Cooled Turbine Blade with Five Internal Cooling Smooth Channels, *Exp. Therm. Fluid Sci.*, *58* (2014), pp. 180-187

[8] Gao, T., *et al.*, Numerical Prediction on Mist/Steam Cooling in a Square Ribbed Channel at Real Gas Turbine Operational Conditions, *Int. J. Heat Mass Trans.*, *108* (2017), pp. 1089-1102

[9] Wang, W., *et al.*, Cooling Performance Analysis of Steam Cooled Gas Turbine Nozzle Guide Vane, *Int. J. Heat Mass Trans.*, *62* (2013), pp. 668-679

[10] Wang, W., *et al.*, Efficiency Study of a Gas Turbine Guide Vane with a Newly Designed Combined Cooling Structure, *Int. J. Heat Mass Trans.*, *80* (2015), pp. 217-226

[11] Shukla, A.K., *et al.*, Performance Evaluation of Steam Injected Gas Turbine Based Power Plant with Inlet Evaporative Cooling, *Appl. Therm. Eng.*, *102* (2016), pp. 454-464

[12] Elwekeel, F.N., *et al.*, Effect of Mist Cooling Technique on Exergy and Energy Analysis of Steam Injected Gas Turbine Cycle, *Appl. Therm. Eng.*, *98* (2016), pp. 298-309
[13] Du, C., *et al.*, Effects of Aerodynamic Parameters on Steam Vortex Cooling Behavior for Gas Turbine Blade Leading Edge, *P. I. MECH. ENG. A-J. POW.*, *230* (2016), 4, pp. 354-365
[14] Kotowicz, J., *et al.*, The Thermodynamic and Economic Characteristics of the Modern Combined Cycle Power Plant with Gas Turbine Steam Cooling, *Energy*, *164* (2018), pp. 359-376
[15] Vadlamudi, T.C., *et al.*, Influence of Different Steam Cooling Techniques for High Pressure Turbine Blades on the Performance of Gas Turbine, *Iranica Journal of Energy & Environment*, *9* (2018), 3, pp. 168-175
[16] Norheim, S., *et al.*, Numerical Investigation of a Radially Cooled Turbine Guide Vane Using Air and Steam as a Cooling Medium, *Computation*, *9* (2021), 6, pp. 63
[17] Zhao, Z., *et al.*, Numerical Study on Cooling Performance of a Steam-Cooled Blade Based on Response Surface Method, *APPL. SCI-BASEL*, *13* (2023), 11, pp. 6625
[18] Amaral S., *et al.*, Design and Optimization of the Internal Cooling Channels of a High Pressure Turbine Blade Part I: Methodology, *J. Turbomach.*, *132* (2010), 2, pp. 021013
[19] Nekahi, S., *et al.*, A Numerical Approach to the Heat Transfer and Thermal Stress in a Gas Turbine Stator Blade Made of HfB2, *Ceram. Int.*, *45* (2019), 18, pp. 24060-24069
[20] Vaferi, K., *et al.*, Heat Transfer, Thermal Stress and Failure Analyses in a TiB2 Gas Turbine Stator Blade, *Ceram. Int.*, *45* (2019), 15, pp. 19331-19339
[21] Rahimi, J., *et al.*, Stress Analysis of a Second Stage Gas Turbine Blade under Asymmetric Thermal Gradient, *Mech. Ind.*, *20* (2019), 6, pp. 607
[22] Rayapati, S., *et al.*, Gas Turbine Blade Failure Scenario Due to Thermal Loads in Case of Nickel Based Super Alloys, *Materials Today: Proceedings*, *46* (2021), pp. 8119-8126
[23] Cai, L., *et al.*, Thermal-Fluid-Solid Coupling Analysis on the Temperature and Thermal Stress Field of a Nickel-Base Superalloy Turbine Blade, *Materials*, *14* (2021), 12, pp. 3315
[24] Xu, L., *et al.*, An Experimental Research on the Cooling Performance of the Turbine Vane with an Advanced Duplex-Medium Combined Cooling, *Int. J. Heat Mass Trans.*, *79* (2014), pp. 72-81
[25] Xi, L., *et al.*, Study on Flow and Heat Transfer Performance of X-type Truss Array Cooling Channel, *Case Stud. Therm. Eng.*, *26* (2021), pp. 101034
[26] Xu, L., *et al.*, Numerical Prediction of Heat Loss From a Test Ribbed Rectangular Channel Using the Conjugate Calculations, *Int. Commun. Heat. Mass.*, *96* (2018), 98-108.
[27] Yun, Z.O.U., *et al.*, Improving the Mechanical Properties of 304 Stainless Steel Using Waterjet Peening, *Mater. Sci+*, *26* (2020), 2, pp. 161-167
[28] Moghanlou, F.S., *et al.*, Numerical Analyses of Heat Transfer and Thermal Stress in a ZrB2 Gas Turbine Stator Blade, *Ceram. Int.*, *45* (2019), 14, pp. 17742-17750.
[29] Kadir, A., *et al.*, Computational Fluid Dynamic and Thermal Stress Analysis of Coatings for High-Temperature Corrosion Protection of Aerospace Gas Turbine Blades, *Heat Transf.—Asian Re.*, *48* (2019), 6, pp. 2302-2328.
[30] Xi, L., et al., Study on Heat Transfer Performance of Steam-Cooled Ribbed Channel Using Neural Networks and Genetic Algorithms, *Int. J. Heat Mass Tran.*, *127* (2018), pp. 1110-1123

Received: 22.04.2024.
Revised: 26.6.2024.
Accepted: 27.6.2024.